IEEE Access
Multidisciplinary | Rapid Review | Open Access Journal

Received August 17, 2019, accepted August 30, 2019, date of publication September 3, 2019, date of current version September 20, 2019.

Digital Object Identifier 10.1109/ACCESS.2019.2939262

Effective Defect Features Extraction for Laser Ultrasonic Signal Processing by Using Time–Frequency Analysis

ZHENYU ZHU[1], HAO SUI[1], LEI YU[1], HONGNA ZHU[1], (Member, IEEE), JINLI ZHANG[2], AND JIANPING PENG[1]

[1]School of Physical Science and Technology, Southwest Jiaotong University, Chengdu 610031, China
[2]National Key Laboratory of Science and Technology on Blind Signal Processing, Chengdu 610031, China

Corresponding author: Hongna Zhu (hnzhu@swjtu.edu.cn)

This work was supported in part by the National Natural Science Foundation of China under Grant 61405167 and Grant 61771409, and in part by the Fundamental Research Funds for the Central Universities under Grant 2682018GF10 and Grant 2682019LK08.

ABSTRACT The time-frequency analysis (TFA) by wavelet transform is adopted for the laser ultrasonic signal processing, and the effective features extraction of the material defect is obtained. The TFA is adopted here to analyze the laser-generated surface acoustic wave (SAW) signal which contains the defect features, the echo wave features are extracted significantly, especially under the condition of low signal-to-noise rate (SNR). The simulation model by using finite element method (FEM) is set up in an aluminum plate with different surface defect depths in detail, and the defect depths prediction with TFA is also considered. It shows that, without extra denoising process, the echo SAW is extracted significantly in case of defect depths ranging from 0.1mm to 0.9mm at SNR of −3dB by TFA. The TFA for processing the laser ultrasonic signal provides a promising way to get the defect information, with the accuracy increased by 7.9dB in this work, which is extremely meaningful for the ultrasonic signal processing and material evaluation.

INDEX TERMS Time-frequency analysis, laser ultrasonic signal, feature extraction, wavelet transform, signal-to-noise rate.

I. INTRODUCTION

Due to the repaid development of laser and ultrasonic technology, laser ultrasonic technique attracts increasing intention, because it shows multiple advantages of high spatial resolution, fruitful wave modes and high sensitivity etc. [1]–[5]. So far, laser ultrasonic has been widely used in many applications, such as biomedical imaging [6], surface defect detection [7]–[9] and material evaluation [10], [11].

As a promising method for analyzing time-varying non-stationary signals, time-frequency analysis (TFA) is playing vital role in signal processing fields, which can extract the details of the high frequency parts and the low frequency parts of a signal effectively. Especially when the signal is in the condition of low SNRs, the TFA can show excellent ability in defect features extraction. The TFA can be obtained with the Short-time Fourier Transform (STFT) [13], Wigner-Ville distribution [14], wavelet transform (WT) [15] and atomic decomposition [16] et al. And it has been variously applied in the mechanical fault diagnosis [17], [18], signal optimization of communication system etc. [19], [20].

Usually for the laser ultrasonic signal processing, the non-stationarity and nonlinearity features cannot be effectively extracted by conventional time-domain or frequency-domain analysis. In particular, the different frequency parts of the surface waves are enhanced or suppressed by the different depth of the defect, leading to the redistribution of the frequency parts in the corresponding signals [21]. However, due to combining both time-domain and frequency-domain information, the TFA can represent the signal features more clearly. In addition, deep learning-based feature extraction method is a good method for signal processing [22]–[24]. But the TFA method is commonly faster and more efficient for feature extraction, especially, in the case of small samples and insufficient machine performance. It is attracting intensive interests in laser ultrasonic signal processing. Laser ultrasonic testing for detecting plastic deformation by TFA was studied [25]. In 2018, the TFA was used to further effectively enhance the high frequency ultrasonic signal contrast for determining corrosion layer thickness of hollow metallic

The associate editor coordinating the review of this manuscript and approving it for publication was Mengmeng Li.

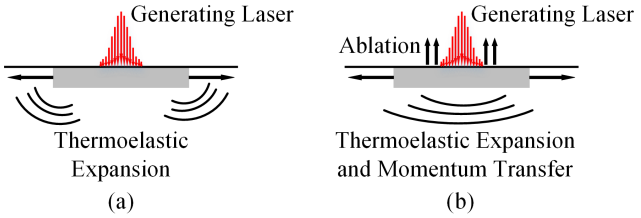

FIGURE 1. The mechanism of laser-generated ultrasonic with (a) thermoelastic mechanism and (b) ablative mechanism.

components [26]. In 2019, the detection and reconstruction of internal defects in a metallic material was performed by means of the TFA of ultrasonic waves [27]. The technique of TFA facilitates the measurement of thickness, Young's modulus, and Poisson's ratio from just one noncontact measurement [28], [29]. However, the noise, which is inevitable in the laser-generated ultrasonic practical system, will hindered the signal processing which result in the defect features cannot be extracted effectively and thus weaken the performance of the defect detecting system. Therefore, it is very necessary to investigate the noises effect on the laser-generated ultrasonic signal processing and extract the defect features effectively for the surface defect detection at practical application.

In this paper, under the condition of low signal-to-noise rate (SNR), TFA method are introduced to analyze the laser ultrasonic signal. As a traditional and mature method for extracting signal features, the TFA is utilized to extract the echo wave of ultrasonic directly without extra denoising process and algorithm improvement, which results in the obvious accuracy enhancement of the surface defect features extraction and paving a way for the defect prediction. The reminder of this paper is organized as follows. In Section II, the principle of laser ultrasonic is given and its finite element method (FEM) model is set up in an aluminum plate, then the surface defects detection and its feature extraction by surface acoustic wave (SAW) with FEM is discussed. In Section III, the TFA by wavelet transform is analyzed, and the application of TFA on laser ultrasonic signal processing for defect features extraction in different cases is investigated in detail, then the defect depths prediction by TFA is also considered. The conclusions are given in Section IV.

II. THERORY AND MODEL

A. PRINCIPLE AND THEORY OF LASER ULTRASONIC

The mechanism of laser-generated ultrasound is shown in Fig. 1. The local, pulsed laser beam impinges on the material, temperature rises due to part of the laser energy is absorbed by the surface layer of the material. And with the transmission of absorbed energy to the surrounding area, a transient non-uniform temperature field is then formed, which leads to the thermal expansion and then results in local vibration and ultrasonic wave generation. The whole process is accompanied by the energy conversion from light to thermal and then to acoustic. There are two mechanisms of laser-generated ultrasonic, which are thermoelastic mechanism (as seen in Fig. 1 [a]) and ablative mechanism (in Fig. 1 [b]), respectively [30].

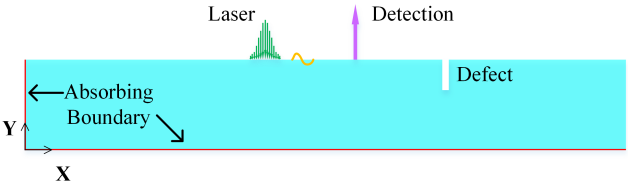

FIGURE 2. The FEM model of laser-generated ultrasonic in aluminum plate.

The optical intensity variation with depth inside an absorbing medium, which is illuminated by a light beam at normal incidence, is given by an exponential decay relation [30]:

$$I(x, y, z, t) = I_0(x, y, t) \exp(-\gamma z) \tag{1}$$

where $I(x, y, t)$ is the incident intensity distribution at the surface, γ is an absorption coefficient characteristic of the material for the given wavelength.

The optical energy absorbed by the material leads to a distributed heat source in the material, which can be expressed as [30]:

$$q(x, y, z, t) = q_0(x, y, t)\gamma \exp(-\gamma z) \tag{2}$$

where q_0 is proportional to I_0 and has the same spatial and temporal properties as the incident laser source.

Generally, the thermoelastic mechanism is mainly used for the practical non-destructive testing. For simplicity, a fully decoupled linear analysis for homogeneous and isotropic materials is considered. And the heat conduction equation in the material can be deduced by establishing the differential equation according to the heat balance condition. Combined with the displacement equation it can be written as [5], [30]:

$$\frac{k}{c_{th}^2}\frac{\partial^2 T}{\partial t^2} + \rho C \frac{\partial T}{\partial t} = k\nabla^2 T + q \tag{3}$$

$$\mu\nabla^2 U + (\lambda + \mu)\nabla(\nabla \cdot U) = \rho\ddot{U} + \beta\nabla T \tag{4}$$

where k, c_{th}, ρ and C are the thermal conductive coefficient, thermal wave velocity, material density and the specific heat capacity, respectively. T and U are transient temperature, vectoral displacement field, respectively. λ and μ are lame coefficient of the material, β is the thermoelastic coupling coefficient defined as:

$$\beta = (3\lambda + 2\mu)\alpha_T \tag{5}$$

where α_T is the thermal expansion coefficient.

B. ESTABLISHMENT OF THE FEM MODEL

The laser ultrasonic technique is mainly applied to detection the metal material defects, of which the aluminum is one of the typical metal. Thus, an aluminum plate is adopted for the model establishment and simulation in our work. Fig. 2 is an aluminum plate model with the size of 0.1 m × 0.015 m, in which the absorption boundary on the bottom surface and the left side can reduce the intensity of the reflected wave dramatically.

TABLE 1. The properties of aluminum used in FEM.

Physical properties	Aluminum
Density (Kg·m^{-3})	2703
Young's modulus (Pa)	7.02×10^{10}
Poisson's Ratio	0.34
Expansion Coeff alpha (K^{-1})	2.31×10^{-5}
Conductivity (W·m^{-1}·K^{-1})	292.6 T<200
	249.5-0.085×T 200≤T≤730
	198.47-0.014×T 730≤T≤T $_{max}$
Specific Heat (J·Kg^{-1}·K^{-1})	3.971×T T<200
	780.27+0.488×T 200≤T<T $_{max}$

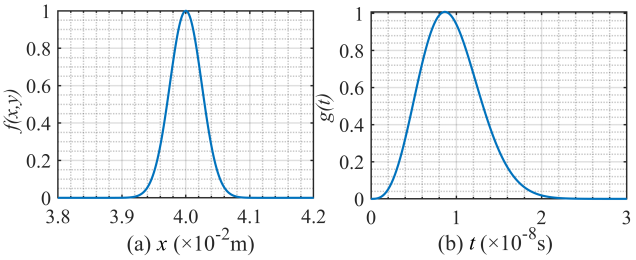

FIGURE 3. (a) Spatial and (b) temporal distribution of simulated gaussian laser pulse.

The parameters of the aluminum plate used in the simulation are explored in Table 1. The Gaussian pulsed laser is located 40 mm to the left side. The heat flux energy formed by laser irradiation on the material surface can be described as [5]:

$$q = E_0 A f\,(x)\, g\,(t) \tag{6}$$

where E_0 is laser intensity at the incident center, A is the absorption rate of material surface, q is total energy absorbed by the material surface. $f\,(x)$ and $g\,(t)$ are the spatial and temporal distribution of the laser pulse, respectively, which can be written as:

$$f\,(x) = \frac{2}{R_G\sqrt{2\pi}} exp(-\frac{(x-x_G)^2}{R_G^2}) \tag{7}$$

$$g\,(t) = \frac{8t^3}{t_0^4} exp(-\frac{2t^2}{t_0^2}) \tag{8}$$

where t_0 is the rise time, R_G is the half width of the laser in the direction x, and x_G is the coordinates of the laser center. Here, the parameters used are: $t_0 = 1\times10^{-8}$ s, $R_G = 1\times10^{-3}$ m, and $x_G = 4\times10^{-2}$ m. Hence, as shown in Fig. 3, the spatial and temporal distribution of the laser pulse is obtained.

The velocity of each waveform by the FEM can be derived as follows [31]:

$$C_L = \sqrt{\frac{E}{\rho}}\sqrt{\frac{1-\sigma}{(1+\sigma)(1-2\sigma)}} \tag{9}$$

$$C_S = \sqrt{\frac{E}{\rho}}\sqrt{\frac{1}{2(1+\sigma)}} \tag{10}$$

$$C_R = \frac{0.87+1.13\sigma}{1+\sigma} C_S \tag{11}$$

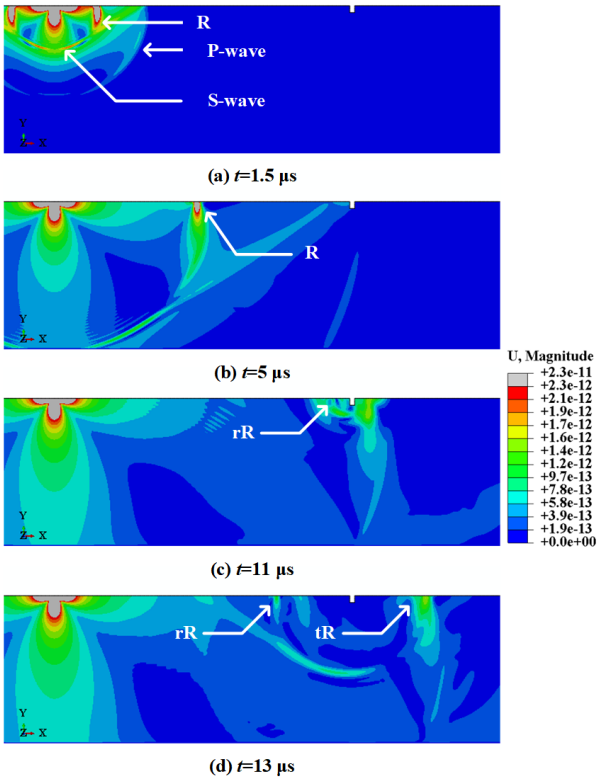

FIGURE 4. The propagation and distribution of laser-generated ultrasonic with time of (a) t = 1.5 μs, (b) t = 5 μs, (c) t = 11 μs and (d) t = 13 μs.

where C_L, C_S, and C_R are the velocity of longitudinal waves, shear wave and surface wave, respectively. E and σ are Young's modulus, Poisson's ratio of the material, respectively.

In this paper, the surface defect is set up by FEM, where its width is fixed to 0.5mm and depth varies from 0.1 mm to 0.9 mm. The defect is located 30 mm to the right side of the laser point source. For detecting the vertical displacement of the surface, a receiving point is set at 15mm to the left side of the defect, as can be seen from Fig. 2. Furthermore, the generated SAW signal propagates from the excitation center to the other regions, and it can be received by the receiving point for the first time. After meeting the surface defect, the SAW propagates continuedly and be reflected partly, then the echo wave signal is received.

C. THE LASER ULTRASONIC SIMULATION WITH FEM

Based on the previous analysis, the FEM of laser ultrasonic in aluminum plate is established. The propagation and distribution of various ultrasonic waves modes is illustrated in Fig. 4. It should be mentioned that the SAW is sensitive to surface defects during its propagation on the material surface. When the SAW encounters a defect, part ultrasonic wave is reflected (defined as rR wave) with wave mode be converted, and the others (defined as tR wave) continue to propagate through the defect, as shown in Fig. 4 (c) and (d). The existence of defect influences the propagation of ultrasonic wave greatly.

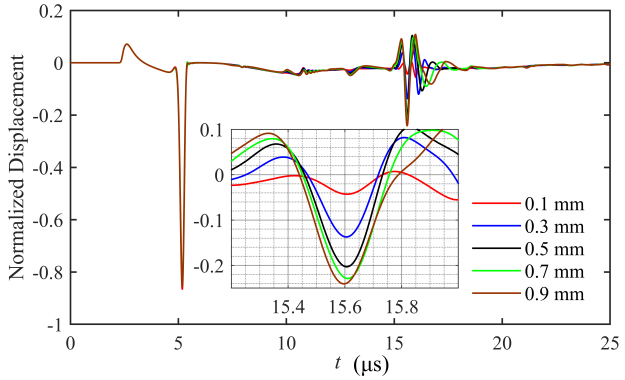

FIGURE 5. The evolution of normalized displacement of echo wave signal with time for different defect depths; the zoom-in view of echo wave amplitude.

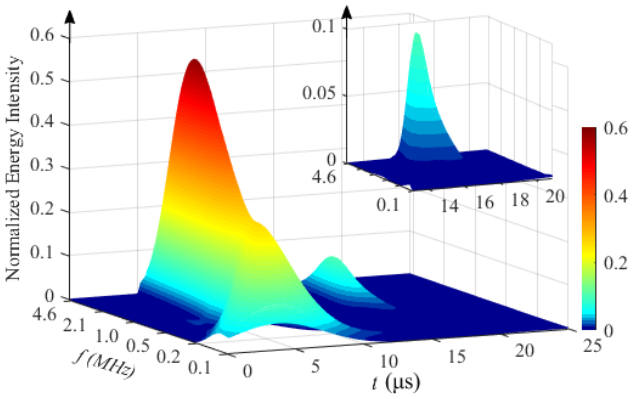

FIGURE 6. The distribution of normalized energy intensity by TFA of the surface defect with depth of 0.7 mm.

The multiple ultrasonic modes are excited by laser, including the longitudinal wave (P-wave), transverse wave (S-wave) and Rayleigh wave (R). P-wave have the fastest speed but lowest energy, S-wave with energy concentration direction of 60 degrees to the surface of the material. And the R, that is SAW, with the slowest speed and only propagated on the surface.

Note that the echo wave signal at the receiving point is a critical parameter for the defect information analysis. Thus, we further investigate the normalized vertical displacement of the echo wave signal in detail, which is described in Fig. 5. In this case, we obtain the initial SAW at $t = 5.2$ μs, and receive the echo wave signal at $t = 15.6$ μs. Based on the arrival time of initial SAW, the propagation velocity of the SAW in the aluminum plate is calculated with $C_{R1} = 2894.6$ m/s, when the relative position between the excitation point and receiving point is fixed. According to the (11), we calculate the theoretical value of $C_{R2} = 2913.7$ m/s. The relative error of simulation is only 0.6% compared to the theory calculation. It also can be seen from Fig. 5, that the normalized displacement of echo wave increases with the increase of the defect depths. Especially, the normalized displacement increases obviously in the case of low depth, due to the echo wave signal is less sensitive to depth variations when the defect depth increases to the equivalent value with the SAW wavelength. Thus, the correctness of the model is demonstrated.

III. LASER ULTRASONIC SIGNAL PROCESSING WITH WAVELET TRANSFORM

A. WAVELET TRANSFORM

The wavelet transform is a suitable TFA method for laser ultrasonic signal processing. The wavelet transform is a time and frequency localized analysis method with fixed window but changeable shape and scale, which defined in time-domain is as follows [15]:

$$W(a,b) = \frac{1}{\sqrt{a}} \int_{-\infty}^{+\infty} f(t) h^*_{a,b}(t) dt \tag{12}$$

where a is scale factor, b is time shift factor and $f(t)$ is the signal function, respectively. $h_{a,b}(t)$ is named as mother wavelet, it can be obtained with different a and b [15]:

$$h_{a,b}(t) = \frac{1}{\sqrt{a}} h(\frac{t-b}{a}) \tag{13}$$

where h is a square integral function, thus the C_h can be written as [15]:

$$C_h = \int dy \, |y|^{-1} \left|\hat{h}(y)\right|^2 < \infty \tag{14}$$

and b can also be expressed as the position of the wavelet in the $h_{a,b}(t)$, while the dilation parameter a governs its frequency. Conversely, for $|a| \gg 1$, the wavelet $h_{a,b}(t)$ is spread out greatly and gets most low frequencies. Hence, the wavelets are a useful way in the case of where better time-resolution at high frequencies than at low frequencies is desirable [15]. Therefore, the wavelet transform is used for TFA to analyze the signal of laser ultrasonic.

B. THE TFA FOR LASER ULTRASONIC

In the following, the TFA by the wavelet transform is performed on the laser ultrasonic signal processing. The signal distribution of the energy intensity, frequency and time is obtained at the receiving point. And because of the time domain resolution of the TFA is inversely proportional to the frequency domain resolution, so the appropriate parameters are selected to ensure that the time domain and frequency domain resolution of the TFA images are in a good state with a reasonable processing speed. Fig. 6 describes TFA image with the defect depth of 0.7 mm. Here, the x-axis represents time, the y-axis is frequency, and the z-axis is normalized spectrum energy intensity for each location. As can be seen from Fig. 6, there appears two clear peaks in the total range of time, the highest peak (with location of 5.3, 1.25, 0.5726), indicates the initial SAW, and the lower peak is echo of SAW (with location of 15.8, 1.42, 0.0924), where the intensity of echo wave is very lower than that of original SAW. Note that the echo SAW can determine the defect information significantly, then we should extract the echo wave information clearly.

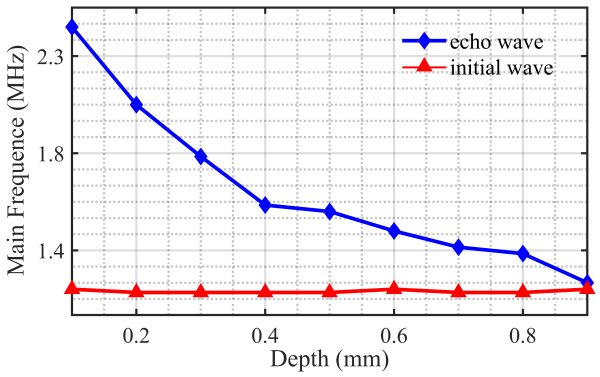

FIGURE 7. The main frequency of echo wave (blue curve) and initial wave (red curve) as the function of defect depth.

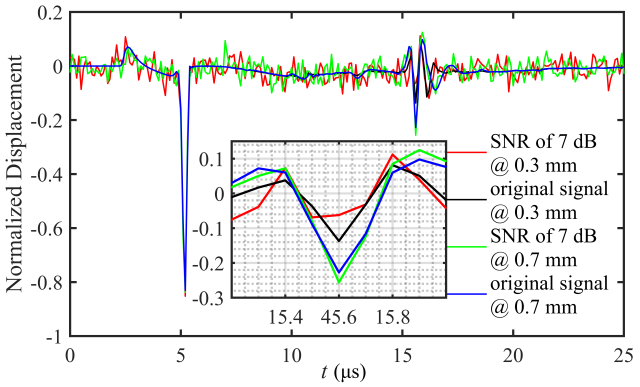

FIGURE 8. A scan of SAW with original signal at defect depth of 0.3 mm (black curve) and of 0.7 mm (green curve) and SAW with SNR of 7 dB at defect depth of 0.3 mm (red curve) and of 0.7 mm (blue curve), zoom-in view of echo wave.

Meanwhile, the variation of main frequency for initial wave and echo wave with different defect depths is illustrated in Fig. 7. The defect depth is in the range of 0.1 mm to 0.9 mm. The main frequency of initial wave maintains 1.25 MHz. However, the main frequency of echo wave varies from 2.5 MHz to 1.2 MHz. Also, the main frequency of echo wave reduces rapidly in the case of lower defect depth from 0.1mm to 0.4mm. This interesting variation of the echo wave main frequency provides another useful solution for the feature extraction of the defect.

In practice, the received ultrasonic signal in the real situation is always accompanied with different types of noises. Usually in the case of low SNRs, it is difficult to effectively extract the defect information. Here, the Gaussian white noise is added to the signal of different defect depths, we thereby compare the influence of the noises on the SAW. It can be seen from the Fig. 8, the defect depth is fixed to 0.3 mm and 0.7 mm, the normalized displacement of the SAW with the original signal and the SNR of 7 dB is illustrated. And the SNR is defined as follows:

$$SNR = \frac{P_{signal}}{P_{noise}} = (\frac{A_{signal}}{A_{noise}})^2 \tag{15}$$

where P and A is the average power and amplitude of the wave.

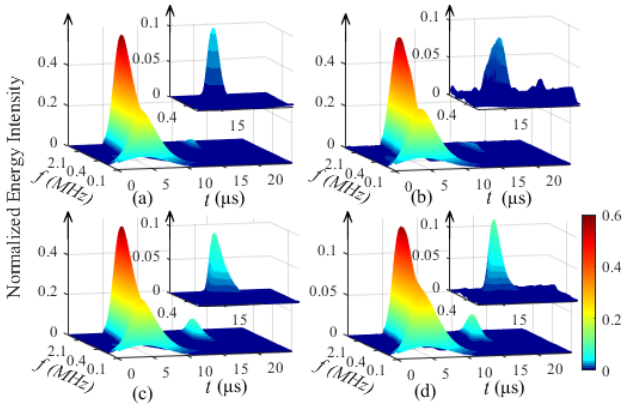

FIGURE 9. The SAW distribution by TFA in case of the defect with depth of (a) 0.3 mm for original signal, (b) 0.3 mm with SNR of 7 dB, (c) 0.7 mm for original signal and (d) 0.7 mm with SNR of 7 dB, zoom-in view of echo wave.

The amplitude of the echo signal is changed obviously when considering the noises influence. When the defect depth is 0.3 mm, the normalized echo amplitude varies from 0.06 to 0.14. But in the case of defect depth of 0.7 mm, the variation is different with that of 0.3 mm. Thus, the defect features cannot be extracted by this time-domain analysis (sometimes named as A scan in field of ultrasonic signal processing) because of the noises influence.

According to the previous analysis, the time-domain analysis cannot represent the depth characteristics of surface defects well, where the defect features cannot be distinguished from the noises in this way. Therefore, we present utilizing the TFA to further analyze the above four cases for getting better defect information, as shown in Fig. 9.

As shown in Fig. 9 (a) and (c), the signal information by TFA with defect depths of 0.3 mm and 0.7 mm are illustrated. There are obvious peak occurs at $t = 5.3\ \mu$s and $t = 15.3\ \mu$s, which represent the initial wave and the echo wave signal of SAW, respectively. As shown in Fig. 9 (b) and (d) on the right, it clearly shows that even when one-dimensional signal is influenced by noises, clutter can also appear in TFA. The echo wave can still be seen from TFA chart compared with one-dimensional signal. And some simple transformations of TFA images can render TFA plane image.

Fig. 10 is the top view of Fig. 9, which further indicates the echo wave information by TFA significantly, as a result, the TFA inhibits obvious defect features extraction from another aspect. It can be seen that, the SAW signal occurs clearly in the range of correct time and frequency. Also, both the frequency and temporal of echo wave broadens with the increase of defect depths, this broaden tendency relating to the defect depth provides another way for defect information analysis.

C. EXTRACTION OF DEFECT FEATURES WITH DIFFEENT SNRS BY TFA

Next, based on previous method, we further discuss the optimization result of TFA for laser ultrasonic defect features extraction in the case of different SNRs.

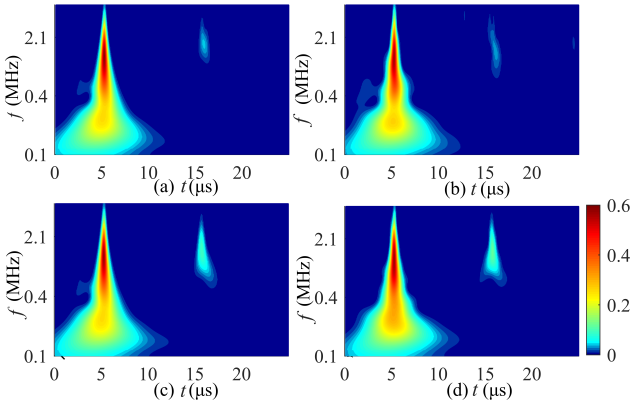

FIGURE 10. The top view of TFA image in case of the defect with depth of (a) 0.3 mm for the original signal, (b) 0.3 mm for the SNR of 7 dB, (c) 0.7 mm for the original signal, and (d) 0.7 mm for the SNR of 7 dB.

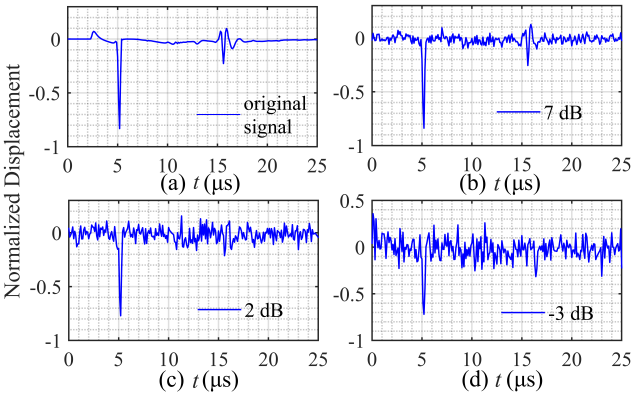

FIGURE 11. The SAW distribution with defect depth of 0.7 mm when the SNR of (a) original signal, (b) 7 dB, (c) 2 dB and (d) −3 dB.

Fig. 11 explores the SAW variation under different SNRs, here, the surface defect depth is fixed to 0.7 mm. We can see that, the echo wave signal is gradually submerged by noises with the decrease of SNRs, in addition, the echo wave cannot be extracted when the SNR is less than 2 dB. This time-domain analysis method cannot distinguish the defect information in this condition.

Consequently, the TFA is introduced for further defect signal processing. The TFA results of the previous four cases are given in Fig. 12. Compared with the time-domain results in Fig. 11, this TFA method illustrates both the initial and the echo wave significantly, with the echo characteristics maintaining unchanged. Despite of the different noises, we can still find two distinct peaks (i.e. representing the initial and echo wave) in the range of 1.25 MHz to 2.5 MHz. That is to say, the TFA can effectively extract the defect properties of materials in practical application, which offering a good solution for non-stationary signals processing.

In addition, based on the TFA technique given previously, we analyze the SAW information with different defect depths. The results are compared between the original signal and

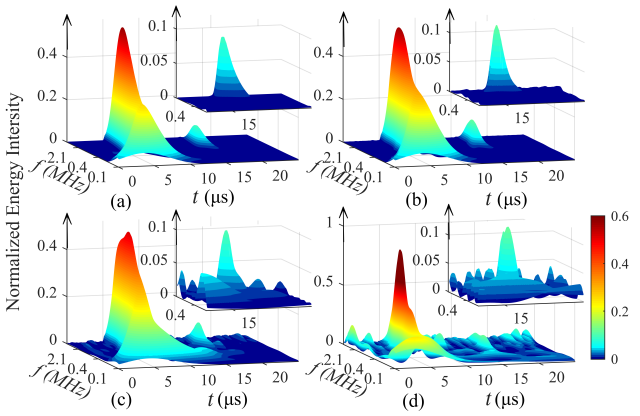

FIGURE 12. The TFA results of Fig. 11.

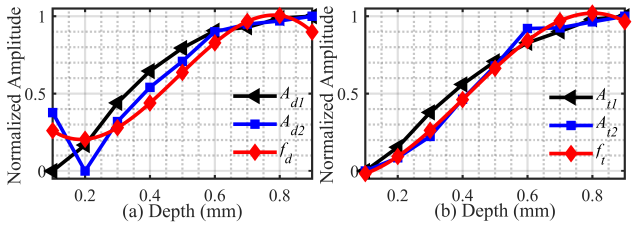

FIGURE 13. The evolution of A_1 (black curve), A_2 (blue curve) and f (red curve) of different defect depths (a) without TFA, and (b) with TFA.

the SNR of −3 dB. Here, we define A_{d1} and A_{t1} is the normalized amplitude of the echo wave for original signal without and with TFA, respectively. A_{d2} and A_{t2} is for the SNR of −3 dB without and with TFA where the echo wave cannot be extracted by time-domain analysis. Subsequently, the values of normalized amplitudes at different defect depths is obtained by TFA. As shown in Fig. 13, the black solid curve explores the variation of the original signal, and the blue solid curve is the one in case of SNR of −3 dB. We then utilize cubic equation to attain the fitting curve of A_{d2} and A_{t2}, as shown with the red curve in Fig. 13. The fitting equation can be induced as:

$$f_d = -0.00798x^3 + 0.116x^2 - 0.3501x - 0.514 \quad (16)$$

$$f_t = 0.004525x^3 + 0.05603x^2 - 0.02589x - 0.04205 \quad (17)$$

The root means square error (*RMSE*), which is an effective parameter for evaluating deviation, is used to express the results between the fitted value and the actual value. It can be written as:

$$RMSE = \sqrt{\frac{1}{m}\sum_{i=1}^{m}(f(i) - A_1(i))^2} \quad (18)$$

It can be calculated that the *RMSE* with TFA is −24.9dB, and the *RMSE* without TFA is −17.0dB, where the *RMSE* value is relative lower than that without the TFA. That is to say, the application of TFA to extract defect features directly can reduce the error by 7.9dB compared to that of without

this method. Thus, the TFA is suitable for the processing of the defect depths prediction and material properties analysis.

IV. CONCLUSION

In summary, by introducing the TFA as suitable signal processing method, the defect features extraction in the laser ultrasonic signal processing is obtained. The results show that the defects features is extracted effectively by using the wavelet transform for TFA, especially at low SNRs. In concrete, the laser-generated ultrasonic is simulated by FEM with establishing the model in aluminum plate, and the propagation and distribution of SAW is explored. Besides, the main frequency of initial and echo SAW by wavelet transform is obtained, as a result, the main frequency of initial wave maintains 1.25 MHz and the main frequency of echo wave deduces with the increase of the defect depths. Also, in the case of different defect depths, the defect features can be extracted by TFA both for original signal and the SNR of 7 dB, the result indicate that the different SNRs do not affect the echo wave frequency and the echo wave broadens with the increase of the defect depths. Under the condition of further decreasing the SNRs, the effective defect features extraction is also achieved by TFA, compared to the time-domain analysis which cannot extract the defect information at low SNRs. In addition, the fitting equation for different defect depths is deduced with TFA and the accuracy increased by 7.9dB. Hence, the TFA method is the alternative and promising tools for laser ultrasonic signal processing to promote the defect feature analysis efficiency, which is an excellent candidate for material evaluation and signal processing at widespread fields in the future.

REFERENCES

[1] R. M. White, "Generation of elastic waves by transient surface heating," *J. Appl. Phys.*, vol. 34, no. 12, pp. 3559–3567, Dec. 1963.
[2] I. A. Viktorov, *Rayleigh and Lamb Waves*. New York, NY, USA: Plenum, 1967, pp. 51–66.
[3] C. Ni, Y. Shi, Z. Shen, J. Lu, and X. Ni, "An analysis of angled surface-breaking crack detection by dual-laser source generated ultrasound," *NDT E Int.*, vol. 43, no. 6, pp. 470–475, Sep. 2010.
[4] B. Xu, Z. Shen, X. Ni, and J. Lu, "Numerical simulation of laser-generated ultrasound by the finite element method," *J. Appl. Phys.*, vol. 95, no. 2, pp. 2116–2122, Jan. 2004.
[5] Y. Zhong, X. Gao, L. Luo, Y. Pan, and C. Qiu, "Simulation of laser ultrasonics for detection of surface-connected rail defects," *J. Nondestruct. Eval.*, vol. 36, no. 4, p. 70, Sep. 2017.
[6] T. Wu, M. Kobayashi, M. Tanabe, and C. H. Yang, "The use of flexible ultrasound transducers for the detection of laser-induced guided waves on curved surfaces at elevated temperatures," *Sensors*, vol. 17, no. 6, p. 1285, Jun. 2017.
[7] W. Zeng, H. Wang, G. Tian, and G. Hu, "Application of laser ultrasound imaging technology in the frequency domain based on Wigner–Ville algorithm for detecting defect," *Opt. Laser Technol.*, vol. 74, pp. 72–78, Nov. 2015.
[8] S. Choi and K. Y. Jhang, "Internal defect detection using laser-generated longitudinal waves in ablation regime," *J. Mech. Sci. Technol.*, vol. 32, no. 9, pp. 4191–4200, Sep. 2018.
[9] Y. Orphanos, K. Kosma, E. Kaselouris, N. Vainos, V. Dimitriou, M. Bakarezos, M. Tatarakis, N. A. Papadogiannis, "Integrated nanosecond laser full-field imaging for femtosecond laser-generated surface acoustic waves in metal film-glass substrate multilayer materials," *Appl. Phys. A, Solids Surf.*, vol. 125, no. 4, p. 269, Mar. 2019.
[10] M. Li, A. M. Lomonosov, Z. Shen, H. Seo, K.-K. Jhang, V. E. Gusev, and C. Ni, "Monitoring of thermal aging of aluminum alloy via nonlinear propagation of acoustic pulses generated and detected by lasers," *Appl. Sci.*, vol. 9, no. 6, p. 1191, Mar. 2019.
[11] S.-P. Tseng, C.-H. Wu, and C.-H. Yang, "Fast inversion calculation for full-field measurement of material properties with laser ultrasound technique," *Phys. Procedia*, vol. 70, pp. 510–513, Jan. 2015.
[12] S. Qian and D. Chen, "Joint time-frequency analysis," *IEEE Signal Process. Mag.*, vol. 16, no. 2, pp. 52–67, Mar. 1999.
[13] P. D. Welch, "The use of fast Fourier transform for the estimation of power spectra: A method based on time averaging over short, modified periodograms," *IEEE Trans. Audio Electroacoust.*, vol. 15, no. 2, pp. 70–73, Jun. 1967.
[14] B. Boashash and P. Black, "An efficient real-time implementation of the Wigner-Ville distribution," *IEEE Trans. Acoust., Speech, Signal Process.*, vol. ASSP-35, no. 11, pp. 1611–1618, Nov. 1987.
[15] I. Daubechies, "The wavelet transform, time-frequency localization and signal analysis," *IEEE Trans. Inf. Theory*, vol. 36, no. 5, pp. 961–1005, Sep. 1990.
[16] F. Jaillet and B. Torrésani, "Time-frequency jigsaw puzzle: Adaptive multiwindow and multilayered Gabor expansions," *Int. J. Wavelets Multiresolut. Inf. Process.*, vol. 5, no. 2, pp. 293–315, Mar. 2007.
[17] X. Chen and Z. Feng, "Time-frequency analysis of torsional vibration signals in resonance region for planetary gearbox fault diagnosis under variable speed conditions," *IEEE Access*, vol. 5, pp. 21918–21926, 2017.
[18] X. Qin, P. Wang, Y. Liu, G. Sheng, and X. Jiang, "Research on distribution network fault recognition method based on time-frequency characteristics of fault waveforms," *IEEE Access*, vol. 6, pp. 7291–7300, 2018.
[19] Q. Lv and H. Qin, "An improved method based on time-frequency distribution to detect time-varying interference for GNSS receivers with single antenna," *IEEE Access*, vol. 7, pp. 38608–38617, 2019.
[20] J. Wang, Z. Mo, H. Zhang, and Q. Miao, "A deep learning method for bearing fault diagnosis based on time-frequency image," *IEEE Access*, vol. 7, pp. 42373–42383, 2019.
[21] M. J. Gómez, C. Castejon, and J. C. Garcia-Prada, "Review of recent advances in the application of the wavelet transform to diagnose cracked rotors," *Algorithms*, vol. 9, no. 1, p. 19, Mar. 2016.
[22] Q. Xuan, Z. Chen, Y. Liu, H. Huang, G. Bao, and D. Zhang, "Multiview generative adversarial network and its application in pearl classification," *IEEE Trans. Ind. Electron.*, vol. 66, no. 10, pp. 8244–8252, Oct. 2019.
[23] Y. Liu, C. Yang, Z. Gao, and Y. Yao, "Ensemble deep kernel learning with application to quality prediction in industrial polymerization processes," *Chemometrics Intell. Lab. Syst.*, vol. 174, pp. 15–21, Mar. 2018.
[24] Y. Liu, Y. Fan, and J. Chen, "Flame images for oxygen content prediction of combustion systems using DBN," *Energy Fuels*, vol. 31, no. 8, pp. 8776–8783, Jul. 2017.
[25] L. Channels, D. Chakraborty, D. Simon, N. Kovvali, J. Spicer, A. Papandreou-Suppappola, D. Cochran, P. Peralta, and A. Chattopadhyay, "Ultrasonic sensing and time-frequency analysis for detecting plastic deformation in an aluminum plate," *Proc. SPIE*, vol. 6926, Apr. 2008, Art. no. 69260P.
[26] H. Liu, L. Zhang, H. F. Liu, S. Chen, S. Wang, Z. Zheng, and K. Yao, "High-frequency ultrasonic methods for determining corrosion layer thickness of hollow metallic components," *Ultrasonics*, vol. 89, pp. 166–172, Sep. 2018.
[27] H. Selim, M. D. Prieto, J. Trull, L. Romeral, and C. Cojocaru, "Laser ultrasound inspection based on wavelet transform and data clustering for defect estimation in metallic samples," *Sensors*, vol. 19, no. 3, p. 573, Jan. 2019.
[28] C. McKee, B. Culshaw, and R. Leach, "Laser ultrasound measurement of diaphragm thickness, Young's modulus and Poisson's ratio in an MEMS device," *IEEE J. Sel. Topics Quantum Electron.*, vol. 23, no. 2, pp. 37–44, Mar./Apr. 2017.
[29] T. Dehoux, N. Tsapis, and B. Audoin, "Relaxation dynamics in single polymer microcapsules probed with laser-generated GHz acoustic waves," *Soft Matter*, vol. 8, no. 9, pp. 2586–2589, Jan. 2012.
[30] S. Krishnaswamy, *Theory and Applications of Laser-Ultrasonic Techniques*. Boca Raton, FL, USA: CRC Press, 2003, pp. 436–448.
[31] Y. Zhan, J. Xue, and C. Liu, "Numerical simulation of laser ultrasonic elastic constant measurement based on abaqus," *Chin. J. Lasers*, vol. 42, no. 5, May 2015, Art. no. 508002.

ZHENYU ZHU received the B.S. degree in electronic information science and technology from Southwest Jiaotong University (SWJTU), Chengdu, China, in 2018, where he is currently pursuing the master's degree with the School of Physical Science and Technology. His research interests include laser ultrasonic and ultrashort pulse technology.

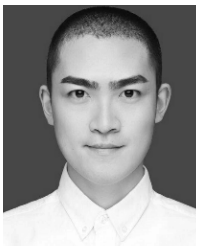

HAO SUI received the B.S. degree in electronic information science and technology from Southwest Jiaotong University (SWJTU), in 2017, where he is currently pursuing the Ph.D. degree. His research interests include laser ultrasonic and signal processing.

LEI YU received the B.S. degree in electronic information science and technology from Southwest Jiaotong University (SWJTU), in 2018, where he is currently pursuing the master's degree. His research interests include distributed fiber sensors and deep learnings.

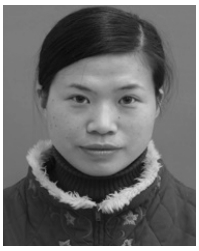

HONGNA ZHU received the master's degree from the National University of Defense, in 2004, and the Ph.D. degree in communication and information system from Southwest Jiaotong University (SWJTU), where she is currently an Associate Professor. She was an Academic Visitor with Swansea University, from 2014 to 2015. She has authored or coauthored more than 60 journals and conference articles, and she is a Candidate of Academic and Technical Leadership of Sichuan Province, China. Her current research interests include optical fiber communication, fiber parametric process, fiber sensors, and nonlinear optics.

JINLI ZHANG received the B.S. degree in physics from Shandong University, in 1998, and the master's degree in electrical engineering from Nanjing University, in 2005. He is currently a Senior Engineer with the National Key Laboratory of Science and Technology on Blind Signal Processing, Chengdu, China. His research interest includes signal processing.

JIANPING PENG was born Sichuan, China, in 1976. He received the Ph.D. degree in electromagnetic field and microwave technology from Southwest Jiaotong University (SWJTU), where he is currently an Associate Professor. His research field covers non-destructive detection in ultrasonic testing, electromagnetic excited thermography and optical image, and photoelectric detection technology and application. He has rich experiences in railway safety with many articles.